Editors' Suggestion Featured in Physics

Discovery of an Exceptionally Strong β-Decay Transition of ^{20}F and Implications for the Fate of Intermediate-Mass Stars

O. S. Kirsebom,[1,2,*] S. Jones,[3,4] D. F. Strömberg,[5,6] G. Martínez-Pinedo,[6,5,†] K. Langanke,[6,5] F. K. Röpke,[4,7] B. A. Brown,[8] T. Eronen,[9] H. O. U. Fynbo,[1] M. Hukkanen,[9] A. Idini,[10] A. Jokinen,[9] A. Kankainen,[9] J. Kostensalo,[9] I. Moore,[9] H. Möller,[6,5] S. T. Ohlmann,[4,11] H. Penttilä,[9] K. Riisager,[1] S. Rinta-Antila,[9] P. C. Srivastava,[12] J. Suhonen,[9] W. H. Trzaska,[9] and J. Äystö[9]

[1]*Department of Physics and Astronomy, Aarhus University, DK-8000 Aarhus C, Denmark*
[2]*Institute for Big Data Analytics, Dalhousie University, Halifax, Nova Scotia B3H 4R2, Canada*
[3]*Computational Physics (XCP) Division, Los Alamos National Laboratory, New Mexico 87545, USA*
[4]*Heidelberger Institut für Theoretische Studien, D-69118 Heidelberg, Germany*
[5]*Institut für Kernphysik (Theoriezentrum), Technische Universität Darmstadt, D-64289 Darmstadt, Germany*
[6]*GSI Helmholtzzentrum für Schwerionenforschung, D-64291 Darmstadt, Germany*
[7]*Zentrum für Astronomie der Universität Heidelberg, Institut für Theoretische Astrophysik, D-69120 Heidelberg, Germany*
[8]*National Superconducting Cyclotron Laboratory, Michigan State University, East Lansing, Michigan 48824, USA*
[9]*Department of Physics, University of Jyväskylä, P.O. Box 35, FI-40014 University of Jyväskylä, Finland*
[10]*Division of Mathematical Physics, Department of Physics, LTH, Lund University, P.O. Box 118, S-22100 Lund, Sweden*
[11]*Max Planck Computing and Data Facility, D-85748 Garching, Germany*
[12]*Department of Physics, Indian Institute of Technology, Roorkee 247667, India*

(Received 22 May 2019; revised manuscript received 15 August 2019; published 24 December 2019)

A significant fraction of stars between 7 and 11 solar masses are thought to become supernovae, but the explosion mechanism is unclear. The answer depends critically on the rate of electron capture on ^{20}Ne in the degenerate oxygen-neon stellar core. However, because of the unknown strength of the transition between the ground states of ^{20}Ne and ^{20}F, it has not previously been possible to fully constrain the rate. By measuring the transition, we establish that its strength is exceptionally large and that it enhances the capture rate by several orders of magnitude. This has a decisive impact on the evolution of the core, increasing the likelihood that the star is (partially) disrupted by a thermonuclear explosion rather than collapsing to form a neutron star. Importantly, our measurement resolves the last remaining nuclear physics uncertainty in the final evolution of degenerate oxygen-neon stellar cores, allowing future studies to address the critical role of convection, which at present is poorly understood.

DOI: 10.1103/PhysRevLett.123.262701

Stars of 7–11 solar masses ($M_\odot$) are prevalent in the Galaxy, their birth and death rates comparable to that of all heavier stars combined [1]. Yet, the ultimate fate of such “intermediate-mass stars” remains uncertain. According to current models [2–4], a significant fraction explode, but the mechanism is a matter of ongoing debate [5–8]. The answer—gravitational collapse or thermonuclear explosion—depends critically on the rate of electron capture on ^{20}Ne in the stellar core. However, because of the unknown strength of the transition between the ground states of ^{20}Ne and ^{20}F, it has not previously been possible to constrain this rate in the relevant temperature-density regime [9]. Here we report on the first measurement of this transition, provide the first accurate determination of the capture rate, and explore the astrophysical implications.

Intermediate-mass stars that undergo central carbon burning become super–asymptotic giant branch stars [1] with a degenerate oxygen-neon (ONe) core consisting mainly of ^{16}O and ^{20}Ne, with smaller amounts of ^{23}Na and ^{24,25}Mg. We are interested in the scenario where the ONe core is able to increase its mass gradually and approach the Chandrasekhar limit, $M_{\rm Ch} \sim 1.37\ M_\odot$. This can occur if nuclear burning continues long enough outside the core or if the core, having lost its outer layers, becoming a white dwarf (WD), is able to accrete material from a binary companion star. As the core approaches $M_{\rm Ch}$, it contracts and warms up, but only gradually, as the heating from compression is balanced by cooling via the emission of thermal neutrinos. The density, on the other hand, rises rapidly, eventually triggering a number of electron-capture processes that greatly influence the temperature evolution of the core. First, the core is cooled by cycles of electron capture followed by β decay on the odd-mass nuclei ^{25}Mg and ^{23}Na [10]. At higher densities, the core is cooled by another such cycle on ^{25}Na, and heated by double electron captures on the even-mass nuclei ^{24}Mg and ^{20}Ne, which produce substantial energy in the second capture. Electron capture on ^{24}Mg occurs first at lower densities due to its smaller Q value, but ^{24}Mg is depleted before the temperature can reach the threshold for oxygen ignition ($T \sim 10^9$ K). Instead, oxygen is ignited by electron capture on ^{20}Ne at somewhat higher densities. Previous studies [5–7,10–14] have considered that electron capture on ^{20}Ne at such conditions proceeds mainly by the allowed transition from the ground state in ^{20}Ne to the first 1^+ state in ^{20}F, which requires a central density of the stellar core of $\rho_{9,c} \approx 9.8$ ($\rho_9 \equiv \rho/10^9$ g cm^{-3}), but it was recently argued [9] that electron capture on ^{20}Ne can start at much lower densities of $\rho_{9,c} \approx 6.8$ via the second-forbidden, nonunique, $0^+ \to 2^+$ transition connecting the ground states of ^{20}Ne and ^{20}F. However, owing to the transition's unknown strength, it was not possible to determine its impact [11]. The onset of electron capture on ^{20}Ne heats the central region, producing a large temperature gradient, which by itself would drive convection but that is counteracted by the composition gradient, which has a stabilizing effect. Stellar models are therefore sensitive to the treatment of convection [5,6,11, 15,16] and electron screening [7,11], predicting central oxygen ignition densities in the range $\rho_{9,c}^{\rm ign} \approx 8.9$–15.8.

The fate of the star—gravitational collapse or thermonuclear explosion—is sensitive to the competition between electron capture and nuclear energy generation. If the ignition of oxygen occurs below some critical central density $\rho_c^{\rm crit}$, oxygen burning releases sufficient energy to reverse the collapse and completely or partially disrupt the star in a thermonuclear explosion [8]. If it occurs above $\rho_c^{\rm crit}$, the deleptonization behind the burning front is so rapid that the loss in pressure cannot be recovered by nuclear burning. Therefore, the collapse continues to nuclear densities, resulting in the birth of a neutron star and the ejection of the stellar envelope [17,18]. Stability analyses based on spherically symmetric simulations predict $\rho_{9,c}^{\rm crit} = 8.9$ [19], though such one-dimensional simulations are able to produce thermonuclear explosions at $\rho_{9,c} \approx 10$ if the flame propagates fast enough [20]. In fact, multidimensional simulations are necessary to model the flame propagation, as the efficiency of the thermonuclear combustion is set by nonlinear instabilities and turbulence that govern the flame propagation speed. Implementing such effects in numerical schemes is very challenging. 2D simulations predict $\rho_{9,c}^{\rm crit} = 7.9$–8.9 [21], while 3D simulations still produce thermonuclear explosions at these densities [8]. Because of the nonlinear nature of the physical processes involved, the outcome should be highly sensitive to the initial conditions. From simulations of thermonuclear supernovae in carbon-oxygen WDs [22], we expect the geometry and the location of the ignition region to have a significant impact on the evolution of the flame morphology. Indeed, 2D simulations just above the critical density no longer predict collapse if oxygen is ignited off center [21].

This illustrates that precise knowledge of the ignition conditions is critical for determining the fate of these intermediate-mass stars. Therefore, the strength of the second-forbidden transition connecting the ground states of ^{20}Ne and ^{20}F was determined through the measurement of the transition's branching ratio in the β decay of ^{20}F. Here we briefly summarize the main aspects of the measurement; details are given in an accompanying paper [23]. The measurement was performed at the JYFL Accelerator Laboratory in Jyväskylä, Finland, using a low-energy radioactive ^{20}F beam from the IGISOL-4 facility [24,25]. Singly charged ^{20}F$^+$ ions were produced by bombarding a BaF_2 target with 6-MeV deuterons. The ions were accelerated to 30 keV, separated according to their mass-to-charge ratio, and guided to the experimental station where they were implanted in a thin carbon foil. The detection system consisted of a Siegbahn-Slätis type intermediate-image magnetic electron transporter [26] combined with a segmented plastic-scintillator detector. The magnetic transporter served to focus the high-energy electrons from the forbidden ground-state transition into the detector while suppressing the intense flux of γ rays and lower-energy electrons due to the allowed transition to the first-excited state in ^{20}Ne, and hence eliminating $\beta\gamma$ summing and $\beta\beta$ pileup as sources of background. Meanwhile, the segmentation of the detector allowed for highly efficient rejection (99.72%) of the cosmic-ray background, while a baffle was used to prevent positrons from reaching the detector. Finally, a $LaBr_3$(Ce) detector was used to measure the 1.63-MeV γ ray associated with the allowed transition, ensuring overall normalization of the measurement.

The allowed β spectra of ^{20}F and ^{12}B and monoenergetic conversion electrons from a ^{207}Bi source were used to characterize the acceptance window of the magnetic transporter and the response of the plastic-scintillator detector for electron energies up to 8.0 MeV. This permitted the detection efficiency of the forbidden transition to be determined directly from the experimental data with a precision of 16%. The response was further modeled with a GEANT4 simulation [27,28], and good agreement was achieved between the measured and simulated energy distributions. For the measurement of the forbidden transition, data were collected for 105 h, with the magnet tuned to focus electrons with energies of ~ 6 to 7 MeV, and background data were collected for 183 h without a beam, but with the magnet still on. The β spectra obtained in these long measurements are displayed in Fig. 1. The forbidden transition (end-point energy of 7.025 MeV) gives rise to excess counts between 5.6 and 6.8 MeV, while the 5 orders of magnitude more intense allowed transition to the first-excited state in ^{20}Ne (end-point energy of 5.391 MeV) dominates at lower energies.

The statistically significant detection of a signal was established through a maximum likelihood fit in which the shapes of the allowed and forbidden transitions were

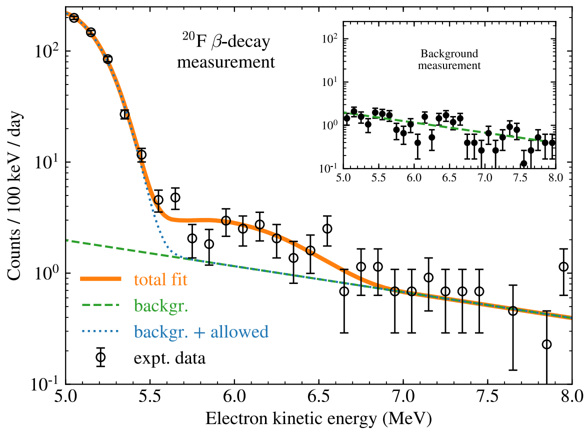

FIG. 1. β spectrum obtained with the magnetic transporter set to select the high-energy tail of the forbidden ground-state transition in the β decay of ^{20}F. (Inset) Background spectrum obtained under the same conditions, but without the ^{20}F beam. The spectrum obtained with the beam exhibits a clear excess in the region 5.6–6.8 MeV due to the forbidden transition.

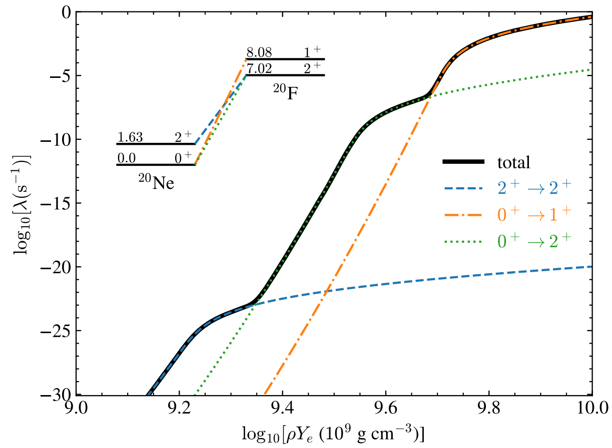

FIG. 2. Astrophysical electron-capture rate as a function of density for a temperature of $T = 0.4$ GK. A simplified level scheme shows the main transitions with the nuclear levels labeled by their spin parity and energy in MeV relative to the ^{20}Ne ground state.

obtained from the GEANT4 simulation, while the shape of the cosmic-ray background was parametrized by an exponential function with two free parameters. Including the forbidden transition in the fit model, we obtained a satisfactory fit quality (p value of 0.080) and constrained the magnitude of the signal with a statistical uncertainty of 19%. In contrast, fitting without the forbidden transition gives an unsatisfactory fit quality (p value of 0.0003). Correcting for the β detection efficiency, normalizing to the total number of decays inferred from the 1.63 MeV γ-ray yield, and adopting the shape factor predicted by our shell-model calculation (see below), we determine the branching ratio to be $0.41(11) \times 10^{-5}$, where systematical and statistical uncertainties have been added in quadrature. Using the known half-life for ^{20}F of 11.0062(80) s [29], we determine the transition strength to be $\log ft = 10.89(11)$. Thus, the transition is 3 orders of magnitude stronger than the only other known second-forbidden, nonunique transition for a nucleus with a similar mass ($^{36}\mathrm{Cl} \rightarrow {}^{36}\mathrm{Ar}$, $\log ft = 13.321(3)$ [30]) and, in fact, one of the strongest of its kind [31].

The electron-capture rate on ^{20}Ne is shown in Fig. 2 for a temperature of $T = 0.4$ GK. Including the forbidden transition, the electron-capture rate increases by up to 8 orders of magnitude in the important density range $\rho_9 \simeq 4.5$–9.5 ($\log_{10}[\rho Y_e (\mathrm{g\,cm^{-3}})] \simeq 9.35$–9.68). As a result, it competes with the timescale of core contraction and affects the evolution of the core. We note that if the strength of the forbidden transition had been similar to what is observed for ^{36}Cl, the electron-capture rate would have been enhanced by "only" 5 orders of magnitude. It would then have remained below the contraction rate, and the forbidden transition would not have been able to affect the evolution of the stellar core.

The electron-capture rate and β-decay rates were calculated following the approach of Ref. [9]. For forbidden transitions, the constant matrix element is replaced by an energy dependent shape factor [32] that is a function of the matrix elements between the initial and final nuclear states. The exact relationship depends on the type of transition. We use the formalism of Refs. [32,33] for β^- and electron capture. The matrix elements are determined from shell-model calculations performed in the sd shell with the USDB interaction [34] using harmonic oscillator single-particle wave functions and constrained by the known strength of the analog $E2$ transition in ^{20}Ne together with the conserved vector current theory. Moreover, we use the bare value of the axial coupling constant since previous calculations of unique second-forbidden transitions have not provided evidence of quenching of the axial coupling constant [35,36]. Our calculations reproduce the observed half-life of the second-forbidden transition to within better than 10%. The matrix elements, rescaled to the observed half-life, are then used for the evaluation of the electron-capture rate taking into account the appropriate kinematics. In this way, we are able to constrain the electron-capture rate to within 25% at the relevant density and temperature conditions, taking into account also the uncertainty on the theoretical shape factor [23].

To quantify the impact of the forbidden transition, we simulate the final evolution of an accreting ONe core using the stellar evolution code MESA [37] following the procedure of Refs. [10,11], where matter is accreted onto the core at a constant rate, $\dot{M}$. We consider the cases $\dot{M}_{-6} = 0.1$, 1.0, and 10 ($\dot{M}_{-6} \equiv \dot{M}/10^{-6}\ M_\odot\ \mathrm{yr}^{-1}$) representative of thermally stable hydrogen burning ($\dot{M}_{-6} \approx 0.4 - 0.7$) [38] and helium burning ($\dot{M}_{-6} \approx 1.5 - 4.5$) [39]. We find that the inclusion of the forbidden transition allows the

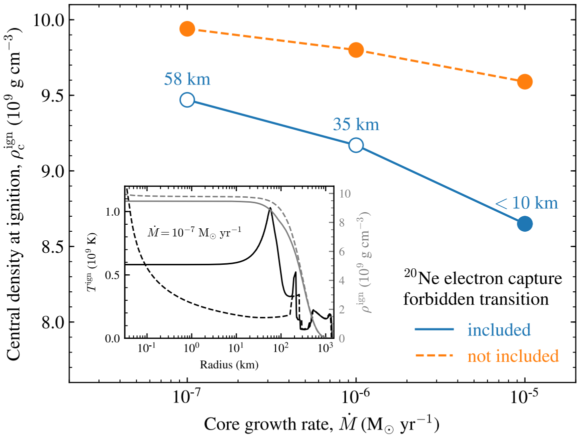

FIG. 3. Central ignition density vs growth rate for a contracting, degenerate ONe core, with and without the forbidden transition between the ground states of ^{20}Ne and ^{20}F. Filled circles denote cases in which oxygen ignition occurs centrally, while empty circles denote off-center ignition at the indicated radius. The panel shows temperature and density profiles at the time of ignition for a low growth rate (10^{-7} $M_\odot$ yr^{-1}).

electron captures on ^{20}Ne to proceed at lower densities (see the Supplemental Material [40]). However, since the forbidden transition is more than 5 orders of magnitude weaker than a typical allowed transition, the captures do not produce a thermal runaway, as would be the case for an allowed transition, but rather a gradual heating of the core. As a result, the star develops an isothermal core with a radius of 10–60 km and, for the $\dot{M}_{-6} = 0.1$ and 1.0 cases, this phase lasts long enough that most ^{20}Ne within the isothermal core is converted to ^{20}O by double electron capture. Hence, further heating occurs in the outer regions of the core triggering an off-center ignition of oxygen. For the $\dot{M}_{-6} = 10$ case, the ignition occurs in a central region with 10 km radius. Figure 3 summarizes the results of our simulations. For all cases considered, the contribution of the forbidden transition leads to earlier heating resulting in oxygen ignition at lower densities. Changes in the chemical composition, in particular the initial amount of ^{24}Mg and ^{25}Mg, affect the evolution somewhat but do not alter the picture qualitatively, unless the ^{24}Mg fraction is made very large [11].

Determining the final outcome after oxygen ignition—gravitational collapse or thermonuclear explosion—requires multidimensional hydrodynamical simulations. We have performed four high-resolution 3D hydrodynamical simulations using the LEAFS code [8,41], with different assumptions for the initial density and flame geometry motivated by the results of the MESA stellar evolution simulations. We also calculate the nucleosynthesis in the ejecta following the approach of Ref. [42]. None of our simulations actually result in core collapse into a neutron star; all are partial thermonuclear explosions that produce a bound remnant consisting of oxygen, neon, and iron-group elements (ONeFe WD). The inclusion of the forbidden transition,

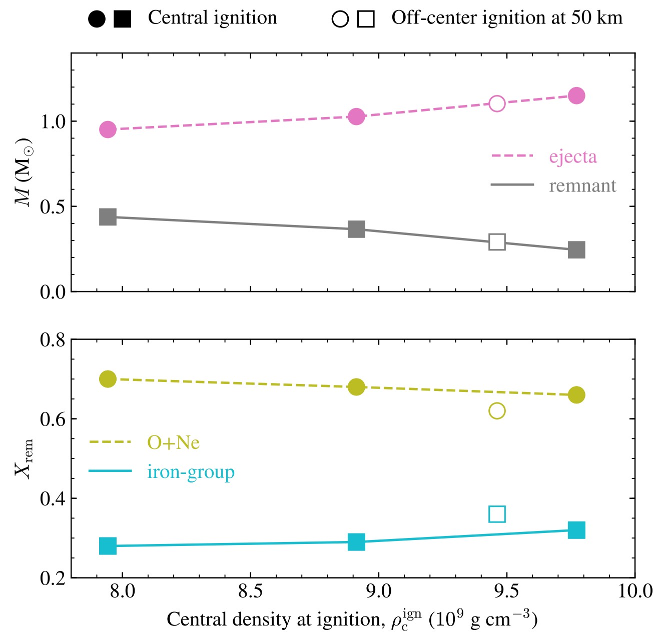

FIG. 4. Mass (M) of bound remnant and ejecta and mass fractions (X) of oxygen + neon and iron-group elements in the remnant are shown as a function of the central density at ignition (ρ_c^{ign}). Filled markers denote simulations with central ignition; empty markers denote simulations with ignition occurring in a sphere with radius of 50 km.

which favors an off-center ignition at lower densities, has a significant impact on the explosion: The lower density slows down the conductive flame and leads to less energetic burning, which results in a more massive remnant because less material is ejected (Fig. 4, top panel). On the other hand, the off-center ignition leads to more energetic burning during the first 1 s of the explosion (see the Supplemental Material [40]), resulting in a higher fraction of iron-group elements in the remnant compared to the centrally ignited models (Fig. 4, bottom panel).

We find that the explosion mechanism has a significant impact on the nucleosynthesis yields. This is primarily due to thermonuclear explosion ejecting far more material, $M_{ej} \sim 1$ $M_\odot$, than the gravitational collapse, $M_{ej} \sim 0.01$ $M_\odot$ [43], although the isotopic distributions also exhibit some differences (Fig. 5), notably in the production factors of ^{50}Ti and ^{54}Cr, which are enhanced by factors of ~20 in the thermonuclear explosion. On the other hand, the changes in ignition density and geometry caused by the forbidden transition have a modest impact on nucleosynthesis, leading to changes of up to ~10% in the production factors of individual isotopes (see the Supplemental Material [40]). We find that the ejecta of the thermonuclear explosion are particularly rich in the neutron-rich isotopes ^{48}Ca, ^{50}Ti, and ^{54}Cr and the trans-iron elements Zn, Se, and Kr (Fig. 5). This has important implications for our understanding of early galactic chemical evolution [42] and may also explain unusual Ti and Cr isotopic ratios found in presolar grains

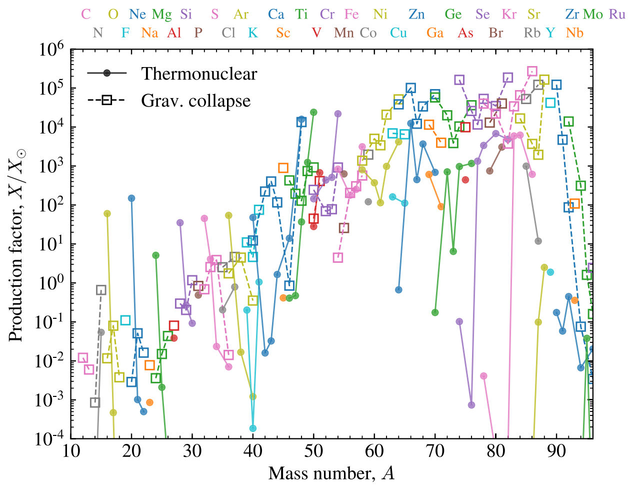

FIG. 5. Mass fraction relative to solar, $X/X_\odot$, of stable isotopes in the ejecta of the (off-center) thermonuclear explosion compared to the gravitational collapse of Ref. [43].

[42,44]. The radionuclide ^{60}Fe is also produced in large amounts ($3.63 \times 10^{-3}\ M_\odot$), implying that the live ^{60}Fe found in deep-sea sediments [45] could have originated from the recent death of a nearby intermediate-mass star [46]. On the other hand, the production of ^{26}Al is rather modest, resulting in a large ^{60}Fe:^{26}Al ratio [42].

In summary, our Letter indicates that the ONe core, for realistic growth rates and composition, will not collapse to a neutron star but rather will be partially disrupted by the oxygen deflagration wave, producing a ONeFe WD and a subluminous type Ia supernova. This is contrary to the commonly accepted view that collapse to a neutron star is more likely [7,21] and has the notable corollary that the Crab Nebula (SN 1054) likely was the result of a low-mass iron core-collapse supernova. Our findings suggest that intermediate-mass stars may be an important (and potentially the only) channel for making ONeFe WDs. Detection or nondetection of such objects with future missions would provide important insight into the explosion mechanism.

The present determination of the electron-capture rate on ^{20}Ne removes the last remaining nuclear physics uncertainty in the evolution of degenerate ONe cores. Not only does the new accurate capture rate result in a reduced ignition density below $\rho_c^{\rm crit}$, it also modifies the initial conditions by causing an off-center ignition. With this result, the most uncertain aspect of the progenitor evolution is whether or not the core becomes convectively unstable [10], and whether the convective energy transport is efficient enough to delay the ignition and the start of the oxygen deflagration wave to densities above the critical density for collapse. Future efforts should therefore focus on characterizing convection in the progenitor evolution. However, the main result of this work will not change: The new accurate ^{20}Ne capture rate tips the balance in favor of a thermonuclear explosion.

This is the first astrophysical case in which a second-forbidden transition has been found to play a decisive role. Our result allows advances in our understanding of the fate of intermediate-mass stars and their contribution to galactic chemical evolution, populations of compact objects in the Universe, and diversity of supernova light curves.

We are indebted to the technical staff at the JYFL Laboratory and Aarhus University for their assistance with refurbishing the spectrometer, and to the members of the IGISOL-4 group for their support during the experiment. This work has been supported by the Academy of Finland under the Finnish Centre of Excellence Programme (Nuclear and Accelerator Based Physics Research at JYFL 2012–2017) and Academy of Finland Grants No. 275389, No. 284516, No. 295207, and No. 312544. This work was supported by the U.S. Department of Energy LDRD program through the Los Alamos National Laboratory. The Los Alamos National Laboratory is operated by Triad National Security, LLC, for the National Nuclear Security Administration of the U.S. Department of Energy (Contract No. 89233218NCA000001). S. J. acknowledges support from a Director's Fellowship at Los Alamos National Laboratory. The work of F. K. R., S. J., and S. T. O. was supported by the Klaus Tschira Foundation, and F. K. R. received additional support through the Collaborative Research Center SFB 881 "The Milky Way System" of the German Research Foundation (DFG). B. A. B. acknowledges the support of NSF Grant No. PHY-1811855, and O. S. K. acknowledges support from the Villum Foundation through Project No. 10117. D. F. S. and G. M.-P. acknowledge the support of the Deutsche Forschungsgemeinschaft (DFG, German Research Foundation), Project No. 279384907–SFB 1245 "Nuclei: From Fundamental Interactions to Structure and Stars"; and the ChETEC COST action (CA16117), funded by COST (European Cooperation in Science and Technology). J. K. acknowledges the financial support of the Jenny and Antti Wihuri Foundation. P. C. S. acknowledges the financial support from the Faculty Initiation Grant (FIG) provided by IIT-Roorkee. A. K. and M. H. acknowledge the support from the European Union's Horizon 2020 research and innovation program under Grant Agreement No. 771036 (ERC CoG MAIDEN).

*Corresponding author.
oliver.kirsebom@dal.ca
†g.martinez@gsi.de

[1] C. L. Doherty, P. Gil-Pons, L. Siess, and J. C. Lattanzio, Pub. Astron. Soc. Aust. **34**, e056 (2017).
[2] A. J. T. Poelarends, F. Herwig, N. Langer, and A. Heger, Astrophys. J. **675**, 614 (2008).
[3] S. Jones *et al.*, Astrophys. J. **772**, 150 (2013).

[4] K. Takahashi, T. Yoshida, and H. Umeda, Astrophys. J. **771**, 28 (2013).
[5] J. Isern, R. Canal, and J. Labay, Astrophys. J. **372**, L83 (1991).
[6] R. Canal, J. Isern, and J. Labay, Astrophys. J. **398**, L49 (1992).
[7] J. Gutiérrez, E. Garcia-Berro, I. Iben, Jr., J. Isern, J. Labay, and R. Canal, Astrophys. J. **459**, 701 (1996).
[8] S. Jones, F. K. Röpke, R. Pakmor, I. R. Seitenzahl, S. T. Ohlmann, and P. V. F. Edelmann, Astron. Astrophys. **593**, A72 (2016).
[9] G. Martínez-Pinedo, Y. H. Lam, K. Langanke, R. G. T. Zegers, and C. Sullivan, Phys. Rev. C **89**, 045806 (2014).
[10] J. Schwab, L. Bildsten, and E. Quataert, Mon. Not. R. Astron. Soc. **472**, 3390 (2017).
[11] J. Schwab, E. Quataert, and L. Bildsten, Mon. Not. R. Astron. Soc. **453**, 1910 (2015).
[12] S. Miyaji, K. Nomoto, K. Yokoi, and D. Sugimoto, Publ. Astron. Soc. Jpn. **32**, 303 (1980).
[13] K. Nomoto, W. M. Sparks, R. A. Fesen, T. R. Gull, S. Miyaji, and D. Sugimoto, Nature (London) **299**, 803 (1982).
[14] K. Nomoto, Astrophys. J. **277**, 791 (1984).
[15] M. Hashimoto, K. Iwamoto, and K. Nomoto, Astrophys. J. **414**, L105 (1993).
[16] N. Tominaga, S. I. Blinnikov, and K. Nomoto, Astrophys. J. **771**, L12 (2013).
[17] F. S. Kitaura, H.-T. Janka, and W. Hillebrandt, Astron. Astrophys. **450**, 345 (2006).
[18] H.-T. Janka, B. Müller, F. S. Kitaura, and R. Buras, Astron. Astrophys. **485**, 199 (2008).
[19] F. X. Timmes and S. E. Woosley, Astrophys. J. **396**, 649 (1992).
[20] K. Nomoto and Y. Kondo, Astrophys. J. **367**, L19 (1991).
[21] S.-C. Leung, K. Nomoto, and T. Suzuki, arXiv:1901.11438.
[22] M. Fink, M. Kromer, I. R. Seitenzahl, F. Ciaraldi-Schoolmann, F. K. Röpke, S. A. Sim, R. Pakmor, A. J. Ruiter, and W. Hillebrandt, Mon. Not. R. Astron. Soc. **438**, 1762 (2014).
[23] O. S. Kirsebom *et al.*, companion paper, Phys. Rev. C **100**, 065805 (2019).
[24] J. Ärje, J. Äystö, H. Hyvönen, P. Taskinen, V. Koponen, J. Honkanen, A. Hautojärvi, and K. Vierinen, Phys. Rev. Lett. **54**, 99 (1985).
[25] I. Moore *et al.*, Nucl. Instrum. Methods Phys. Res., Sect. B **317**, 208 (2013).
[26] R. Julin, J. Kantele, J. Kumpulainen, M. Luontama, V. Nieminen, A. Passoja, W. Trzaska, and E. Verho, Nucl. Instrum. Methods Phys. Res., Sect. A **270**, 74 (1988).
[27] S. Agostinelli *et al.*, Nucl. Instrum. Methods Phys. Res., Sect. A **506**, 250 (2003).
[28] J. Allison *et al.*, Nucl. Instrum. Methods Phys. Res., Sect. A **835**, 186 (2016).
[29] D. P. Burdette, M. Brodeur, T. Ahn, J. Allen, D. W. Bardayan, F. D. Becchetti, D. Blankstein, G. Brown, B. Frentz *et al.*, Phys. Rev. C **99**, 015501 (2019).
[30] A. A. Kriss and D. M. Hamby, Nucl. Instrum. Methods Phys. Res., Sect. A **525**, 553 (2004).
[31] B. Singh, J. L. Rodriguez, S. S. M. Wong, and J. K. Tuli, Nucl. Data Sheets **84**, 487 (1998).
[32] H. Behrens and W. Bühring, *Electron Radial Wave Functions and Nuclear Beta-Decay* (Clarendon, Oxford, 1982).
[33] H. Behrens and W. Bühring, Nucl. Phys. **A162**, 111 (1971).
[34] B. A. Brown and W. A. Richter, Phys. Rev. C **74**, 034315 (2006).
[35] E. K. Warburton, Phys. Rev. C **45**, 463 (1992).
[36] G. Martínez-Pinedo and P. Vogel, Phys. Rev. Lett. **81**, 281 (1998).
[37] B. Paxton *et al.*, Astrophys. J. Suppl. Ser. **234**, 34 (2018).
[38] W. M. Wolf, L. Bildsten, J. Brooks, and B. Paxton, Astrophys. J. **777**, 136 (2013).
[39] J. Brooks, L. Bildsten, J. Schwab, and B. Paxton, Astrophys. J. **821**, 28 (2016).
[40] See Supplemental Material at http://link.aps.org/supplemental/10.1103/PhysRevLett.123.262701 for details on the MESA and LEAFS simulations.
[41] M. Reinecke, W. Hillebrandt, and J. C. Niemeyer, Astron. Astrophys. **391**, 1167 (2002).
[42] S. Jones, F. K. Röpke, C. Fryer, A. J. Ruiter, I. R. Seitenzahl, L. R. Nittler, S. T. Ohlmann, R. Reifarth, M. Pignatari, and K. Belczynski, Astron. Astrophys. **622**, A74 (2019).
[43] S. Wanajo, B. Müller, H.-T. Janka, and A. Heger, Astrophys. J. **852**, 40 (2018).
[44] L. R. Nittler, C. M. O'D. Alexander, N. Liu, and J. Wang, Astrophys. J. Lett. **856**, L24 (2018).
[45] A. Wallner *et al.*, Nature (London) **532**, 69 (2016).
[46] S. Wanajo, H.-T. Janka, and B. Müller, Astrophys. J. Lett. **774**, L6 (2013).